SLAC-PUB-2985
October 1982
(T/E)

ASSESSING QCD IN DEEP-INELASTIC $e\gamma$ SCATTERING*

C. Peterson† and P. M. Zerwas§
Stanford Linear Accelerator Center
Stanford University, Stanford, California 94305
and
T. F. Walsh
Deutsches Elektronensynchrotron, D-2 Hamburg, Germany

ABSTRACT

We consider hadron production in deep inelastic scattering of electrons on photons.

(i) Exploiting the leading order QCD corrections due to gluon bremsstrahlung we find that the photon structure functions rapidly approach their asymptotic form which can be calculated in QCD.

(ii) Replacing QCD by a theory with fixed quark-gluon coupling constant [scalar or Abelian gluons] gives dramatic changes: for Bjorken x away from 0, the asymptotic form of the structure function is scale-invariant, with a shape quite unlike the QCD shape, and the structure function diverges for $x = 0$.

(iii) The pointlike component of the photon gives final state jets emerging at large angles to the axis of the real + virtual photon, in contrast to the hadronic component of the photon.

Submitted to Nuclear Physics B

---

*Work supported in part by the Department of Energy under contract DE-AC03-76SF00515.

†Present Address: NORDITA, Blegdamsvej 17, DK-2100 Copenhagen.

§Kade Fellow, on leave from Technische Hochschule Aachen.

1. INTRODUCTION

It is well-known that deep-inelastic electron-photon scattering

$$e\gamma \to e' + \text{hadrons} \qquad (1)$$

provides an opportunity to measure the photon-structure functions which are predicted by QCD [1-4]. This contrasts with scattering on a nucleon target where only the Q^2 evolution of the structure functions is predicted; the structure functions themselves are not (yet) calculable.

In this paper we expand our earlier work [4] on a number of points. We continue to exploit the zeroth order Born approximation [5] (fig. 1a) and also lowest order QCD via the Altarelli-Parisi equations (fig. 1b). This is adequate to our purposes here. (Higher order QCD corrections to the structure functions themselves have been extensively studied elsewhere [6].)

1.1 Approach to the Asymptotic solutions

Asymptotically the photon-structure function (F_T^γ) increases proportional to $\ell n\ Q^2$ [5,1-4]. Next-to-leading order QCD gives minor corrections to this Q^2 behavior [6]. However, starting from a fairly low Q_0^2, the Altarelli-Parisi equations also give contributions to F^γ which decrease as inverse powers of $\ell n\ Q^2$. These terms have the same general form as for a hadron target. In fact, one might speculate that they originate entirely from the hadronic component of the photon (fig. 1c). Though being negligible asymptotically, we have to assess their impact on F^γ in the present Q^2 range. This question is discussed in section 2. The net effect appears to be small.

1.2 Alternative scenarios

Being renormalizable and asymptotically free, QCD is generally considered to be the only candidate theory of the strong interactions. Nevertheless, one may wonder just how sensitive any phenomenological conclusion is to the essential elements of the theory. For this purpose it is useful to change basic ingredients of the theory in an *ad hoc* way, and examine the resulting effects. In section 3 we consider what would happen if the gluons were scalar or Abelian vectors and if their short-distance coupling to quarks did not run but was simply a small constant. It turns out that the structure function is strongly affected by such an *ad hoc* change. For Bjorken x away from 0, it is asymptotically scale invariant, i.e., does not rise $\propto \ell n\, Q^2$, and it is strongly peaked (diverging) at x = 0, unlike the experimental data.

1.3 Structure of final states

The hadronic event structure reflects the underlying process. The pointlike component of the photon [5,7] gives rise to jets emerging at large angle to the axis of the real and virtual photon in $e\gamma \to e'X$. By contrast, the hadronic component to the photon will give a jet structure predominantly along the collision axis. Large angle jets only emerge as an $\mathcal{O}(\alpha_s)$ effect in this case, forming a triplet of jets. Since the hadronic and pointlike structure of the photon are important at low and high Bjorken x, respectively, we expect the event structure to be x-dependent. We take this up in section 4.

The main background process to inelastic $e\gamma$ scattering is the inelastic Compton effect [4]. A complete final state analysis of this process is found in appendix C.

2. PHOTON STRUCTURE FUNCTIONS

We recapitulate some generalities here for the sake of completeness. The $e\gamma$ cross section for $e^{\pm}(p) + \gamma(k) \to e^{\pm}(p') + X$ is [4]

$$\frac{d\sigma}{dxdyd\phi/2\pi} = \frac{4\pi\alpha^2(kp)}{Q^4}\left[1 + (1-y)^2\right]\left[2xF_T^\gamma + \varepsilon(y)\,F_L^\gamma + \varepsilon(\zeta)\,\varepsilon(y)\,F_X^\gamma\right] \qquad (2)$$

where $x = Q^2/2(kq)$, $y = (kq)/(kp)$, $\zeta = E_\gamma/E_{beam}$ and $\varepsilon(y) = 2(1-y)/[1+(1-y)^2]$, so that $\varepsilon(y)$ and $\varepsilon(\zeta)$ are the degree of polarization of the virtual and real photons; ϕ is the angle between the scattering planes of the small angle and large angle $e^{\pm}$. One often uses the structure function $F_2(x,Q^2)$ and the quark distributions $q(x,Q^2)$,

$$F_2^\gamma(x,Q^2) = 2x\,F_T^\gamma(x,Q^2) + F_L^\gamma(x,Q^2) \qquad (3)$$

$$\begin{aligned} F_2^\gamma(x,Q^2) &\simeq 2x\,F_T^\gamma(x,Q^2) \\ &= x\sum_{fl} e_q^2\left[q(x,Q^2) + \bar{q}(x,Q^2)\right] \end{aligned} \qquad (4)$$

Ignoring strong interactions as a zeroth order Born approximation ($\alpha_s \to 0$) [fig. 1a],

$$\begin{aligned} F_T^\gamma &\simeq \frac{\alpha\langle e^4\rangle}{2\pi}\left[x^2 + (1-x)^2\right]\ln\frac{W^2}{\mu^2} \\ &\xrightarrow[Q^2\to\infty]{} \frac{\alpha\langle e^4\rangle}{2\pi}\left[x^2 + (1-x)^2\right]\ln\frac{Q^2}{\Lambda^2} \\ F_L^\gamma &\simeq \frac{4\alpha\langle e^4\rangle}{\pi}\,x^2(1-x) \\ F_X^\gamma &\simeq -\frac{\alpha\langle e^4\rangle}{\pi}\,x^3 \end{aligned} \qquad (5)$$

where $W^2 = Q^2(1-x)/x$ and $\langle e^4 \rangle = 3 \sum e_q^4$ (sum over flavors). The quark mass is μ, and for light quarks we replace μ by the inverse of the confinement range, $\mu \to \Lambda$. From the above we have

$$q(x,Q^2)_{Born} \simeq 3 e_q^2 \frac{\alpha}{2\pi} \left[x^2 + (1-x)^2 \right] \ell n \frac{Q^2}{\Lambda^2}$$
$$\equiv e_q^2 \, d(x)_{Born} \, \ell n \frac{Q^2}{\Lambda^2} \qquad (6)$$

for each flavor species.

Including gluon radiation gives calculable corrections to $F_{T,L}^{\gamma}(x,Q^2)$ [fig. 1b]. To leading order in α_s the quark and the gluon distributions are given by

$$\frac{\partial q(m,t)}{\partial t} = e_q^2 d(m)_{Born} + \frac{1}{2\pi bt} \left[A_{qq}(m) \, q(m,t) + A_{GG}(m) \, G(m,t) \right]$$
$$\frac{\partial G(m,t)}{\partial t} = \frac{1}{2\pi bt} \left[\sum_{q,\bar{q}} A_{Gq}(m) \, q(m,t) + A_{GG}(m) \, G(m,t) \right] \qquad (7)$$

where the notation is as follows. We write the moments as $q(m,t) = \int dx \, x^{m-1} q(x,t)$ [and similarly for $G(m,t)$], setting $t = \ell n(Q^2/\Lambda^2)$ and $2\pi b = (33-2n_f)/6$. The anomalous dimension matrix A_{ij} is given in appendix A. Equations (7) are solved by a change of variable $s = \ell n(t/t_0)$ for the nonsinglet and singlet moments

$$\Delta(m,s) = q_{2/3}(m,t) - q_{1/3}(m,t)$$
$$\Sigma(m,s) = \sum_{f1} \left[q(m,t) + \bar{q}(m,t) \right] \quad .$$

The solutions for the quark distributions are easily found to be

$$\Delta(m,s) = \Delta(m,0)\ \exp\left\{-\ d_{NS}\, s\right\} + \frac{1}{3}\frac{d(m)_{Born}}{1+d_{NS}}\left[1 - \exp\left\{-\left(1+d_{NS}\right)s\right\}\right]t \qquad (8)$$

$$\Sigma(m,s) = \frac{\exp\left\{\lambda_+ s\right\}\left[-\ G(m,0) + \mu_-\Sigma(m,0)\right] + \exp\left\{\lambda_- s\right\}\left[G(m,0) - \mu_+\Sigma(m,0)\right]}{\mu_- - \mu_+} \qquad (9)$$

$$+ \frac{5n_f}{9}\frac{d(m)_{Born}}{\mu_- - \mu_+}\left(\frac{\mu_-}{1-\lambda_+}\left[1 - \exp\left\{-\left(1-\lambda_+\right)s\right\}\right] - \frac{\mu_+}{1-\lambda_-}\left[1 - \exp\left\{-\left(1-\lambda_-\right)s\right\}\right]\right)t$$

where d_{NS}, $\lambda_\pm$ and $\mu_\pm$ are recorded in appendix B. For large Q^2 they approach the well-known asymptotic values

$$\Delta^\infty(m,s) = \frac{1}{3}\frac{d(m)_{Born}}{1+d_{NS}}\ \ell n\ \frac{Q^2}{\Lambda^2} \qquad (10)$$

$$\Sigma^\infty(m,s) = \frac{5n_f}{9}\frac{d(m)_{Born}}{\mu_- - \mu_+}\left(\frac{\mu_-}{1-\lambda_+} - \frac{\mu_+}{1-\lambda_-}\right)\ell n\ \frac{Q^2}{\Lambda^2} \qquad (11)$$

independent of the initial conditions at $s = 0$.

In contrast to these asymptotic solutions, eqs. (8) and (9) require input values for $q(x,Q_0^2)$ and $G(x,Q_0^2)$ at some reference $Q^2 = Q_0^2$. For low Q_0^2 one expects substantial contributions to the parton densities from the hadronic photon component. [We are not sure though, whether there is any Q_0 at all, even in the $\lesssim$1 GeV range, where the photon is nothing else but a degenerate vector meson.]

The hadronic piece of the photon structure function [fig. 1c] is usually estimated from ρ^o meson dominance [2,4], $|\gamma\rangle_{had} \simeq (e/f_\rho)|\rho\rangle$. Ignoring the small ϕ contribution [s quarks contribute sixteen times less than u quarks] and also the small ω contribution [for $f_\omega^2 = 9f_\rho^2$] we derive

$$F_2(x)_\rho \simeq 2\left[\frac{4}{9}\left(\frac{e}{f_\rho}\right)^2 \frac{1}{2}\, xq(x) + \frac{1}{9}\left(\frac{e}{f_\rho}\right)^2 \frac{1}{2}\, xq(x)\right]$$
$$= \frac{5}{9}\left(\frac{e}{f_\rho}\right)^2 xq(x) \qquad (12)$$

where $q(x)$ is the quark distribution in ρ^o. An estimate of $q(x)$ can be extracted from μ pair production in π-nucleon scattering, with the result that $xq(x) \approx \frac{1}{2}(1-x)$.

In the operator product expansion it is more natural to add the vector mesons ρ,ω coherently.* From

$$|\gamma\rangle_{had} \simeq \frac{e}{f_\rho}|\rho\rangle + \frac{e}{f_\omega}|\omega\rangle + \frac{e}{f_\varphi}|\varphi\rangle$$
$$= \frac{e}{f_\rho}\sqrt{2}\left[\frac{2}{3}|u\bar{u}\rangle - \frac{1}{3}|d\bar{d}\rangle - \frac{1}{3}|s\bar{s}\rangle\right] , \qquad (13)$$

we deduce an increase of the VDM contribution by a factor 1.6,

$$F_2(x)_{had} = \frac{8}{9}\left(\frac{e}{f_\rho}\right)^2 xq(x) \quad . \qquad (14)$$

To assess the influence of the input values on the behavior of the photon structure function in the presently experimentally explored (x,Q^2) domain, we have compared the evolution of quark densities, derived from eqs. (8) and (9), with the variation of their asymptotic form over the Q^2 range from 2 GeV^2 to 100 GeV^2 [9]. At $Q_0^2 = 2$ GeV^2 we used a flat $xq(x,Q_0^2)$ as suggested by PLUTO data and we put $xG(x,Q_0^2) = 0$. [Our results are insensitive to this last assumption.] Falling back upon experimental data for the initial conditions we don't need a detailed picture of the origin of the parton densities at Q_0^2. We show the ratio

*This has also been discussed for large $p_\perp$ physics in ref. [8].

of the full and asymptotic $q_{2/3}(m,Q^2)$ in fig. 2 for $\Lambda^2 = 0.1$ GeV^2. The deviation from the asymptotic behavior is small, even in the low Q^2 range $\lesssim$ 20 to 30%. This renders $e\gamma$ scattering a valuable instrument to explore quantum chromodynamics. In fig. 3 we show the integral of $F_2(x,Q^2)$ together with available data as a function of Q^2.* The experimental data are in reasonable agreement with the QCD prediction across two orders of magnitude in Q^2.

3. ALTERNATIVE SCENARIOS

The Born approximation, generally paraphrased as the parton model prediction, is of course independent of the strong interaction theory considered. The differences between QCD and an alternative scenario appear when gluon radiation is taken into account. One can replace QCD by theories with the scalar gluons or Abelian vector gluons (see, e.g., [10]). Then the anomalous dimensions change; they are listed in appendix A. More important is the choice of a fixed (nonrunning) short-distance coupling. Equations (7) are changed to

$$\frac{\partial q(m,t)}{\partial t} = e_q^2\, d(m)_{\text{Born}} + \frac{\alpha^*}{2\pi}\left[A_{qq}(m)\; q(m,t) + A_{qG}(m)\; G(m,t)\right] \qquad (15)$$

and similarly for $G(x,t)$ [α^* is the small, fixed coupling constant]. These equations are solved by the replacement $s = \ell n(t/t_0) \to t - t_0 = \ell n(Q^2/Q_0^2)$. The solutions for the nonsinglet and singlet distributions are

$$\Delta(m,t) = \Delta\left(m,t_0\right)\, \exp\left\{-d_{NS}\left(t-t_0\right)\right\} + \frac{1}{3}\,\frac{d(m)_{\text{Born}}}{d_{NS}}\left[1 - \exp\left\{-d_{NS}\left(t-t_0\right)\right\}\right] \qquad (16)$$

*This integral contains a nonleading (Q^2 independent) piece which is numerically small. We estimated its magnitude from the nonleading box contribution together with the (low Q^2) integral of eq. (14).

$$\Sigma(m,t) =$$

$$\frac{\exp\{\lambda_+(t-t_0)\}\left[-G(m,t_0)+\mu_-\Sigma(m,t_0)\right]+\exp\{\lambda_-(t-t_0)\}\left[G(m,t_0)-\mu_+\Sigma(m,t_0)\right]}{\mu_- - \mu_+}$$

$$+\frac{5n_f}{9}\,\frac{d(m)_{Born}}{\mu_- - \mu_+}\left(\frac{\mu_+}{\lambda_-}\left[1-\exp\{\lambda_-(t-t_0)\}\right]-\frac{\mu_-}{\lambda_+}\left[1-\exp\{\lambda_+(t-t_0)\}\right]\right). \tag{17}$$

The m dependent coefficients are the same as in appendix B, except that the QCD matrix A_{ij} is replaced by the corresponding values given in the table of appendix A, and $1/2\pi b$ by $\overset{*}{\alpha}/2\pi$. For $\lambda_+(2) = 0$, the first term in the last brackets is to be rewritten as $\mu_-(2)(t-t_0)$. Most interesting is the asymptotic form of the distributions for large Q^2,

$$\Delta^{\infty}(m,t) = \frac{1}{3}\,\frac{d(m)_{Born}}{d_{NS}}$$

$$\Sigma^{\infty}(m>2,t) = \frac{5n_f}{9}\,\frac{d(m)_{Born}}{\mu_- - \mu_+}\left(\frac{\mu_+}{\lambda_-}-\frac{\mu_-}{\lambda_+}\right) \tag{18}$$

and the total quark momentum,

$$\Sigma^{\infty}(m=2,t) = \frac{5n_f}{9}\,\frac{\mu_-(2)\;d(2)_{Born}}{\mu_-(2)-\mu_+(2)}\;\ell n\,\frac{Q^2}{Q_0^2} \tag{19}$$

There is a fundamental difference between QCD and theories with small fixed coupling constants. While in QCD the number of quarks rises uniformly for all x with energy $\propto \ell n(Q^2)$, we find Q^2 independent, scale-invariant quark distributions for all finite x away from 0 in fixed coupling theories. The logarithmically increasing number of quarks in the basic γ splitting $\to q\bar{q}$ before gluon radiation starts, accumulate at $x \to 0$; this is evident from the logarithmic divergence of $\Sigma(2,t)$ in eq. (19). This result is physically plausible. In fixed coupling

theories, the increasing number of quarks from $\gamma \to q\bar{q}$ (Born term) is lost at finite x entirely through gluon bremsstrahlung. In QCD, however, gluon bremsstrahlung is weakened due to the asymptotically decreasing coupling constant. The net result is a well-balanced gain and loss, resulting in just a change of the x shape of the gluon-radiation corrected photon structure function relative to the parton model.

In fig. 4 we compare the asymptotic shapes [with arbitrary normalization] of the 2/3 charge quark distributions in QCD with scalar and Abelian vector gluon theories with fixed coupling constants. It is evident that the asymptotic forms of fixed coupling theories don't match the experimental data [9] of the photon structure function whereas QCD does.

The absolute magnitude of Δ^{∞} and $\Sigma^{\infty}(m>2)$ is $\mathcal{O}(\alpha/\alpha^*)$ while $\Sigma^{\infty}(2,t)$ is independent of α^* [$\alpha << \alpha^*$ of course for eq. (15), et cetera, to be valid]. The strong coupling constant in the denominator is plausible since the weaker gluon bremsstrahlung the larger will be the number of quarks at finite x. As the asymptotic expressions for scalar gluons are simple, we note them explicitly,

$$\frac{\Delta^{\infty}(m)}{\Delta(m,t)_{\text{Born}}} = \frac{4}{1 - \frac{2}{m(m+1)}} \frac{1}{\frac{\alpha^*}{2\pi} \ln \frac{Q^2}{\mu^2}} \quad ,$$

$$\frac{\Sigma^{\infty}(m>2)}{\Sigma(m>2,t)_{\text{Born}}} = \frac{4}{1 - \frac{6}{m(m+1)}} \frac{1}{\frac{\alpha^*}{2\pi} \ln \frac{Q^2}{\mu^2}} \quad ,$$

$$\frac{\Sigma^{\infty}(m=2,t)}{\Sigma(m=2,t)_{\text{Born}}} = \frac{1}{1 + \frac{1}{18n_f}} \quad .$$

Choosing $\alpha^*/2\pi \lesssim 1$, a value required to simulate an $\mathcal{O}(10\%)$ 3-jet rate in e^+e^- annihilation, we find that the Born terms start overshooting the scalar asymptotic forms at $Q^2 = \mathcal{O}(50\ \mathrm{GeV}^2)$.

4. FINAL STATES

The final state from the pointlike term in F_2^γ is distinctive. There will be jets at large angles to the $\gamma\gamma^*$ collision axis (fig. 5a) already in zeroth order of the QCD coupling constant. By contrast, the hadronic piece of the photon will give limited p_T relative to the $\gamma\gamma^*$ collision axis (fig. 5b), plus $\mathcal{O}(\alpha_s)$ corrections which will give a small hard tail to the p_T distribution. We first calculate the Born approximation to the pointlike term.

Including the angular dependence, the cross section for $\gamma\gamma^* \to 2$ jets is defined by three structure functions,

$$\frac{d\sigma}{dxdyd\Omega/4\pi} = \frac{4\pi\alpha^2(kp)}{Q^4}\left[1 + (1-y)^2\right] \times \left[2xF_T(x,z) + \varepsilon(y)\left(1+\frac{1}{2}\cos 2\chi\right)F_L(x,z) + \rho(y)\cos\chi\, F_A(x,z)\right] \tag{20}$$

where $z = \cos\theta$, θ being the polar angle of the jets relative to the $\gamma\gamma^*$ axis in the cms, and χ is the azimuthal angle between the plane formed by the $\gamma\gamma^*$ and jet axes and the (large angle) $e^\pm$ scattering plane;

$$\rho(y) = \frac{(2-y)\sqrt{1-y}}{1+(1-y)^2} \quad .$$

This general structure follows from a helicity analysis of electron scattering processes [11]. The Born term structure functions can easily be derived from the helicity amplitudes for the box diagrams [12],

$$F_T(x,z) = \frac{\alpha\langle e^4\rangle}{\pi}\left[x^2 + (1-x)^2\right]\frac{1+z^2}{1-z^2} \quad ,$$

$$F_L(x,z) = \frac{4\alpha\langle e^4\rangle}{\pi}\, x^2(1-x) \quad , \tag{21}$$

$$F_A(x,z) = \frac{4\alpha\langle e^4\rangle}{\pi}\cdot\frac{z}{\sqrt{1-z^2}}\,(1-2x)\sqrt{x(1-x)} \quad .$$

After integrating over θ we rediscover the transverse and longitudinal structure functions of eq. (5). The z-dependence of $F_i(x,z)$ is shown in fig. 6 for two typical x values.

Transverse momentum distributions relative to the $\gamma\gamma^*$ axis will be of experimental interest. We estimate these, ignoring uncertainties in the axis caused by QCD radiative corrections.

The distribution in jet transverse momenta $p^2_{T,jet} = \frac{1}{4}W^2\sin^2\theta$ follows from eqs. (20) and (21),

$$\left\langle p^2_{T,jet}\right\rangle = \frac{W^2}{4}\,\frac{\int dz\,\frac{1+z^2}{1-z^2}\left(1-z^2\right)}{\int dz\,\frac{1+z^2}{1-z^2}} \tag{22}$$

$$\simeq \frac{1}{3}\,\frac{W^2}{\ell n\, W^2/\Lambda^2}$$

again introducing $\mu^2 \to \Lambda^2$ in the argument of the logarithm. This is shown in fig. 7a.

The single particle p_T^2 spectrum needs an estimate of the nonperturbative effects. Following ref. [13] we take for the produced hadrons in a single event

$$\left\langle p_T^2 \right\rangle = \left\langle p_T^2 \right\rangle_{NP} + \left\langle P_\parallel^2 \right\rangle \sin^2\theta - \frac{1}{2}\left\langle p_T^2 \right\rangle_{NP} \sin^2\theta \qquad (23)$$

where

$$\left\langle p_\parallel^2 \right\rangle = \frac{\int d\xi \left(\xi \frac{W}{2}\right)^2 D_q(\xi)}{\int d\xi\, D_q(\xi)}$$

$$= \frac{W^2}{4} \left\langle \xi^2 \right\rangle$$

ignoring scaling violations in the one-particle fragmentation functions $D_q(\xi)$. Averaging (23) over many events we find

$$\left\langle p_T^2 \right\rangle \simeq \left\langle p_T^2 \right\rangle_{NP} + \frac{1}{3} \frac{\left\langle \xi^2 \right\rangle W^2}{\ell n\, W^2/\Lambda^2} \left[1 - \frac{2\left\langle p_T^2 \right\rangle_{NP}}{\left\langle \xi^2 \right\rangle W^2} \right] \qquad (24)$$

For our estimates we take $\langle p_T^2 \rangle_{NP} = 0.17$ GeV^2 and $\langle \xi^2 \rangle = 0.042$ [13]. The second term in the bracket in eq. (24) is then very small. In fig. 7b we show $\langle p_T^2 \rangle$ as a function of W together with the VDM expectation, $\langle p_T^2 \rangle_{VDM} = \langle p_T^2 \rangle_{NP}$. As expected, the pointlike contribution dominates at large p_T. In fig. 8a we convert this to $\langle p_T^2 \rangle$ as a function of Bjorken x. Large W corresponds to small x where the hadronic piece is important and where gluon bremsstrahlung corrections to the Born approximation should be large. Away from x = 0, we expect that the Born term gives a good first approximation to $\langle p_T^2 \rangle$. Figure 8b shows $\langle p_T^2 \rangle$ at $Q^2 = 100$ GeV^2 weighted by the relative fraction of hadronic and pointlike (Born) cross sections. A considerable increase of $\langle p_T^2 \rangle$ relative to the VDM value is expected at large W.

Acknowledgements

Two of us, C.P. and P.Z., thank S. Drell for the hospitality extended to them at SLAC. We gratefully acknowledge numerous discussions on $\gamma\gamma$ physics with Ch. Berger, S. Brodsky, D. Burke and W. Wagner.

Appendix A

Anomalous dimensions

Moments of parton probabilities for QCD, Abelian-vector gluons and Abelian-scalar gluons (see also [9]). In all cases, quarks are assumed to come in three colors, and the color degrees of freedom are always summed over. We have chosen $n_f = 4$.

	QCD	Abelian Vector Gluons	Abelian Scalar Gluons
$A_{qq}(m)$	$\frac{4}{3}\left[-\frac{1}{2}+\frac{1}{m(m+1)}-2\sum_{2}^{m}\frac{1}{j}\right]$	$-\frac{1}{2}+\frac{1}{m(m+1)}-2\sum_{2}^{m}\frac{1}{j}$	$-\frac{1}{4}\left[1-\frac{2}{m(m+1)}\right]$
$A_{Gq}(m)$	$\frac{4}{3}\ \frac{2+m+m^2}{m\left(m^2-1\right)}$	$\frac{2+m+m^2}{m\left(m^2-1\right)}$	$\frac{1}{2(m+1)}$
$A_{qG}(m)$	$\frac{1}{2}\ \frac{2+m+m^2}{m(m+1)(m+2)}$	$3\ \frac{2+m+m^2}{m(m+1)(m+2)}$	$\frac{3}{m}$
$A_{GG}(m)$	$3\left[-\frac{1}{6}+\frac{2}{m(m-1)}+\frac{2}{(m+1)(m+2)}-2\sum_{2}^{m}\frac{1}{j}-\frac{n_f}{9}\right]$	$-2n_f$	$-3n_f$

Appendix B

Inhomogeneous parton-shower equations

To obtain the solution for $\Sigma(m,s)$, we consider the equations

$$\frac{\partial}{\partial s}\begin{bmatrix}\Sigma(m,s)\\ G(m,s)\end{bmatrix} = \begin{bmatrix}f_B(m,s)\\ 0\end{bmatrix} + \frac{1}{2\pi b}\begin{bmatrix}A_{qq}(m) & 2n_f A_{qG}(m)\\ A_{Gq}(m) & A_{GG}(m)\end{bmatrix}\begin{bmatrix}\Sigma(m,s)\\ G(m,s)\end{bmatrix} \tag{B.1}$$

where

$$f_B(m,s) = \frac{5n_f}{9}\, d(m)_{Born}\, t_0\, e^s$$

$$= \frac{5n_f}{9}\,\frac{\alpha}{2\pi}\,\frac{m^2+m+2}{m(m+1)(m+2)}\, t_0\, e^s$$

The eigenvalues and corresponding eigenvectors are given by*

$$\lambda_\pm = \frac{1}{2}\,\frac{\left(A_{GG}+A_{qq}\right) \pm \sqrt{\left(A_{GG}-A_{qq}\right)^2 + 8n_f\, A_{qG}\, A_{Gq}}}{2\pi b}$$

$$\nu_\pm \propto \begin{bmatrix}\frac{1}{\mu_\pm}\\ 1\end{bmatrix} \tag{B.2}$$

with

$$\mu_\pm = \frac{\left(A_{GG}-A_{qq}\right) \pm \sqrt{\left(A_{GG}-A_{qq}\right)^2 + 8n_f A_{qG} A_{Gq}}}{4n_f A_{qG}} \tag{B.3}$$

They determine the development of the homogeneous part of the differential equations from the initial distributions at $s = 0$,

*Note that $d_{NS} = -A_{qq}/2\pi b$.

$$\Sigma_H(m,s) = \frac{\exp\{\lambda_+ s\}\left[-G(m,0) + \mu_- \Sigma(m,0)\right] + \exp\{\lambda_- s\}\left[G(m,0) - \mu_+ \Sigma(m,0)\right]}{\mu_- - \mu_+} \quad . \quad (B.4)$$

Similarly the inhomogeneous part is given by

$$\Sigma_{IH}(m,s) = \frac{\int_0^s ds' f_B(m,s')\left[\mu_- \exp\{\lambda_+(s-s')\} - \mu_+ \exp\{\lambda_-(s-s')\}\right]}{\mu_- - \mu_+} \quad , \quad (B.5)$$

$$= \frac{5n_f}{9} \frac{d(m)_{Born}\, t_0}{\mu_- - \mu_+}$$

$$\times \left[\frac{\mu_-}{1-\lambda_+}\left(\exp\{s\} - \exp\{\lambda_+ s\}\right) - \frac{\mu_+}{1-\lambda_-}\left(\exp\{s\} - \exp\{\lambda_- s\}\right)\right].$$

This asymptotically leading term is independent of the initial conditions at $s = 0$.

Appendix C

Inelastic Compton process

The inelastic Compton process $e\gamma \to e'\gamma^*$, $\gamma^* \to q\bar{q}$ is the main background to deep inelastic $e\gamma$ scattering. In ref. [4] this background was shown to be controllable. For completeness, we here give the full angular dependence of the cross section.

$$\frac{d\sigma}{dxdydcos\theta d\chi/2\pi} = \frac{\alpha}{2\pi}\,\sigma(M^2)\,\frac{y}{1-y}\left[1+(1-y)^2\right]\left\{\frac{3}{8}\left(1+\cos^2\theta\right)\sigma_T + \frac{3}{4}\sin^2\theta\left[1+\frac{1}{2}\cos 2\chi\right]\varepsilon(y)\,\sigma_L + \frac{3}{4}\sin 2\theta\,\cos\chi\,\sigma_A\right\}, \tag{C.1}$$

where

$$\sigma_T = x^2 + (1-x)^2 \quad ,$$
$$\sigma_L = 2x(1-x) \quad , \tag{C.2}$$
$$\sigma_A = (1-2x)\sqrt{x(1-x)} \quad .$$

$\sigma(M^2)$ is the e^+e^- annihilation cross section at $M^2 = sy(1-x)$. After integrating over θ,χ one recognizes the well-known x,y form of the inelastic Compton cross section.*

*Due to a misprint, a factor (-x) was omitted in the last term within the square bracket of eq. (C3) in ref. [4].

References

[1] E. Witten, Nucl. Phys. B120 (1977) 189.

[2] C. H. Llewellyn Smith, Phys. Lett. 79B (1978) 83;
W. R. Frazer and J. F. Gunion, Phys. Rev. D20 (1979) 147.

[3] R. DeWitt, L. M. Jones, J. Sullivan, D. Willen and H. Wyld, Phys. Rev. D19 (1979) 2046; E., Phys. Rev. D20 (1979) 1751.

[4] C. Peterson, T. F. Walsh and P. M. Zerwas, Nucl. Phys. B174 (1980) 424.

[5] T. F. Walsh and P. M. Zerwas, Phys. Lett. 44B (1973) 195.

[6] W. A. Bardeen and A. J. Buras, Phys. Rev. D20 (1979) 166;
D. W. Duke and J. F. Owens, Phys. Rev. D22 (1980) 2280;
T. Uematsu and T. F. Walsh, Nucl. Phys. B199 (1982) 98.

[7] S. J. Brodsky et al., Phys. Rev. Lett. 41 (1978) 672.

[8] M. Fontannaz et al., Z. Phys. C6 (1980) 241.

[9] Ch. Berger et al., Phys. Lett. 107B (1981) 168;
H. J. Behrend et al., DESY preprint 82-055;
W. Bartel et al., DESY preprint 82-064;
D. Burke, Paris Conference, 1982.

[10] M. Glück and E. Reya, Nucl Phys. B156 (1979) 456;
H. Abramowicz et al., Z. Physik C13 (1982) 199;
W. Bartel et al., DESY 82-060 (1982).

[11] G. Köpp, R. Maciejko and P. M. Zerwas, Nucl. Phys. B144 (1978) 123.

[12] G. Köpp, T. F. Walsh and P. M. Zerwas, Nucl. Phys. B70 (1974) 46.

[13] P. Hoyer, P. Osland, H. Sander, T. F. Walsh and P. M. Zerwas, Nucl. Phys. B161 (1979) 349.

Figure Captions

Fig. 1. Three different contributions to the photon structure function:
a) quark-pair production;
b) QCD corrections to (a);
c) hadronic contribution, $\gamma = \rho, \omega, \phi, \ldots$ (VDM) .

Fig. 2. Ratio of the full to the asymptotic QCD solution for $q_{2/3}(m,Q^2)$; the quark distrubutions are assumed to be flat at $Q_0^2 = 2$ GeV^2 and the gluon component is neglected there; $\Lambda^2 = 0.1$ GeV^2.

Fig. 3. Integrated $F_2(x,Q^2)$ in QCD compared with data from ref. [9]. Notice that the data include cuts lowering the value of the integral by $\mathcal{O}(20\%)$.

Fig. 4. Asymptotic quark distributions for QCD, a scalar and an Abelian vector gluon theory; also shown is the common Born term. Normalization is arbitrary.

Fig. 5. Final state jets of inelastic $e\gamma$ scattering in the $\gamma\gamma^*$ cms:
a) pointlike, and
b) VDM mechanisms.

Fig. 6. $z = \cos\theta$ dependence of F_T, F_L and F_A [eq. (21)] for:
a) $x = 0.2$, and
b) $x = 0.8$.

Fig. 7. a) $\langle p_T^2 \rangle$ for an emerging jet as a function of W in $e\gamma \to eq\bar{q}$;
b) $\langle p_T^2 \rangle$ for a single hadron as a function of W from the Born term and the VDM contributions, respectively.

Fig. 8. a) $\langle p_T^2 \rangle$ for a single hadron as a function of Bjorken x at $Q^2 = 10$ and 100 GeV^2 from the Born term and VDM contributions, respectively.

b) $\langle p_T^2 \rangle$ for a single hadron as a function of x at $Q^2 = 100$ GeV^2 weighted by the Born term and VDM contributions.

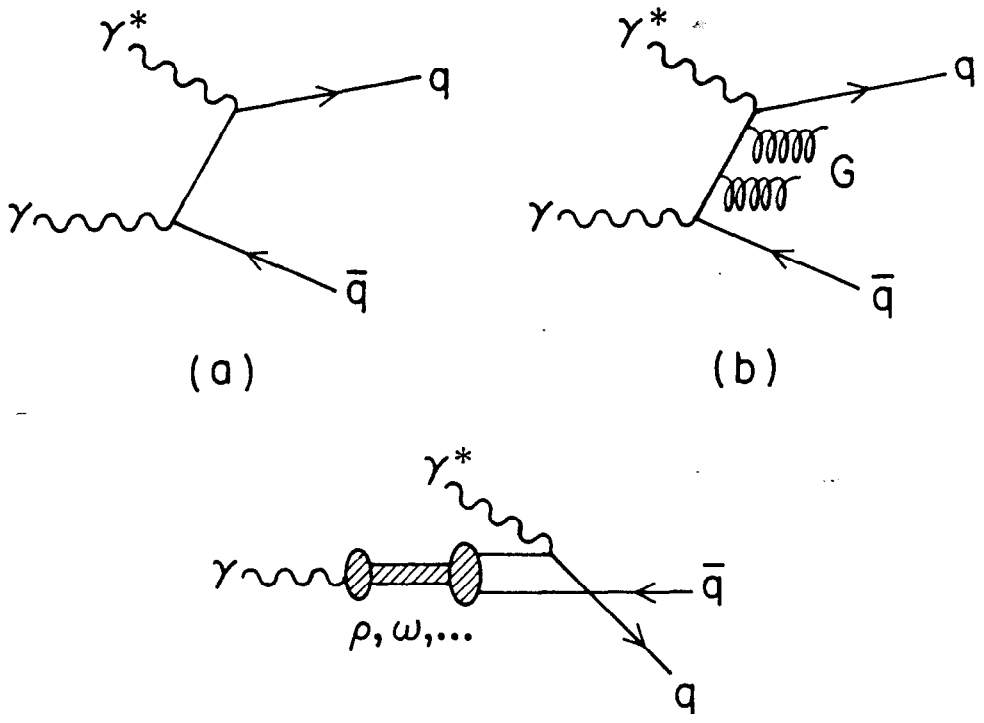

10-82

4392A1

Fig. 1

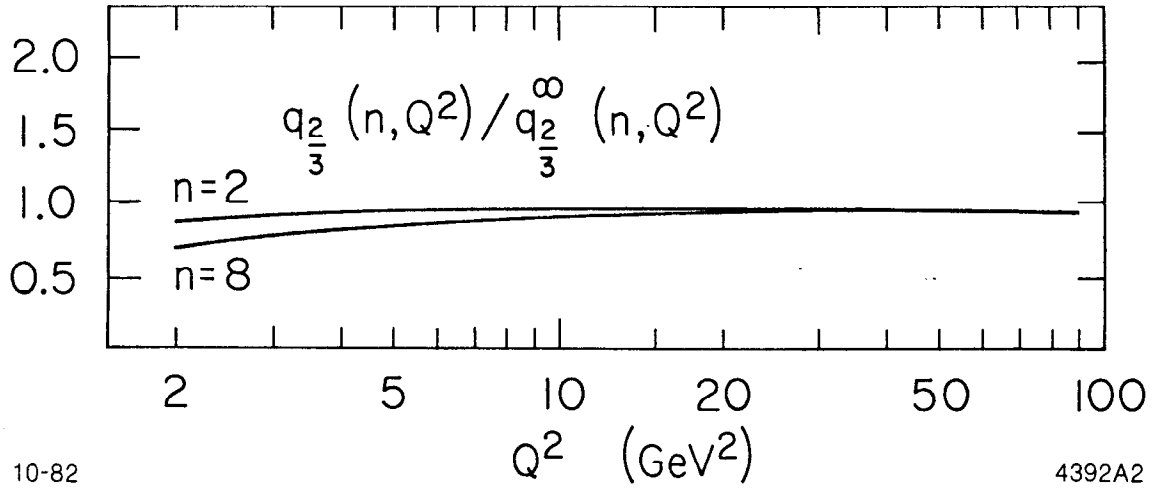
2.0
1.5
1.0
0.5
$q_{\frac{2}{3}}(n,Q^2)/q_{\frac{2}{3}}^{\infty}(n,Q^2)$
n=2
n=8
2
5
10
20
50
100
Q^2 (GeV^2)
10-82
4392A2

Fig. 2

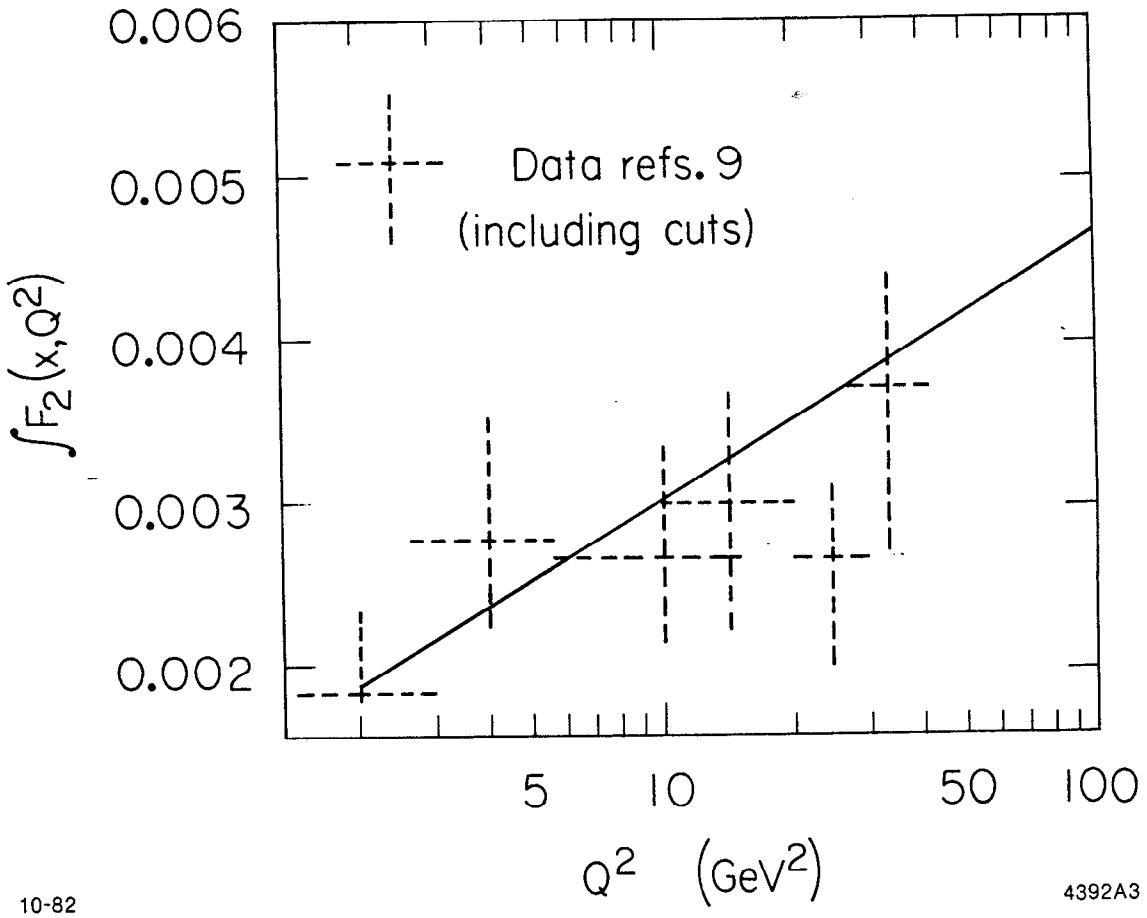
0.006
0.005
0.004
0.003
0.002
$\int F_2(x,Q^2)$
Data refs. 9
(including cuts)
5
10
50
100
Q^2 (GeV^2)
10-82
4392A3

Fig. 3

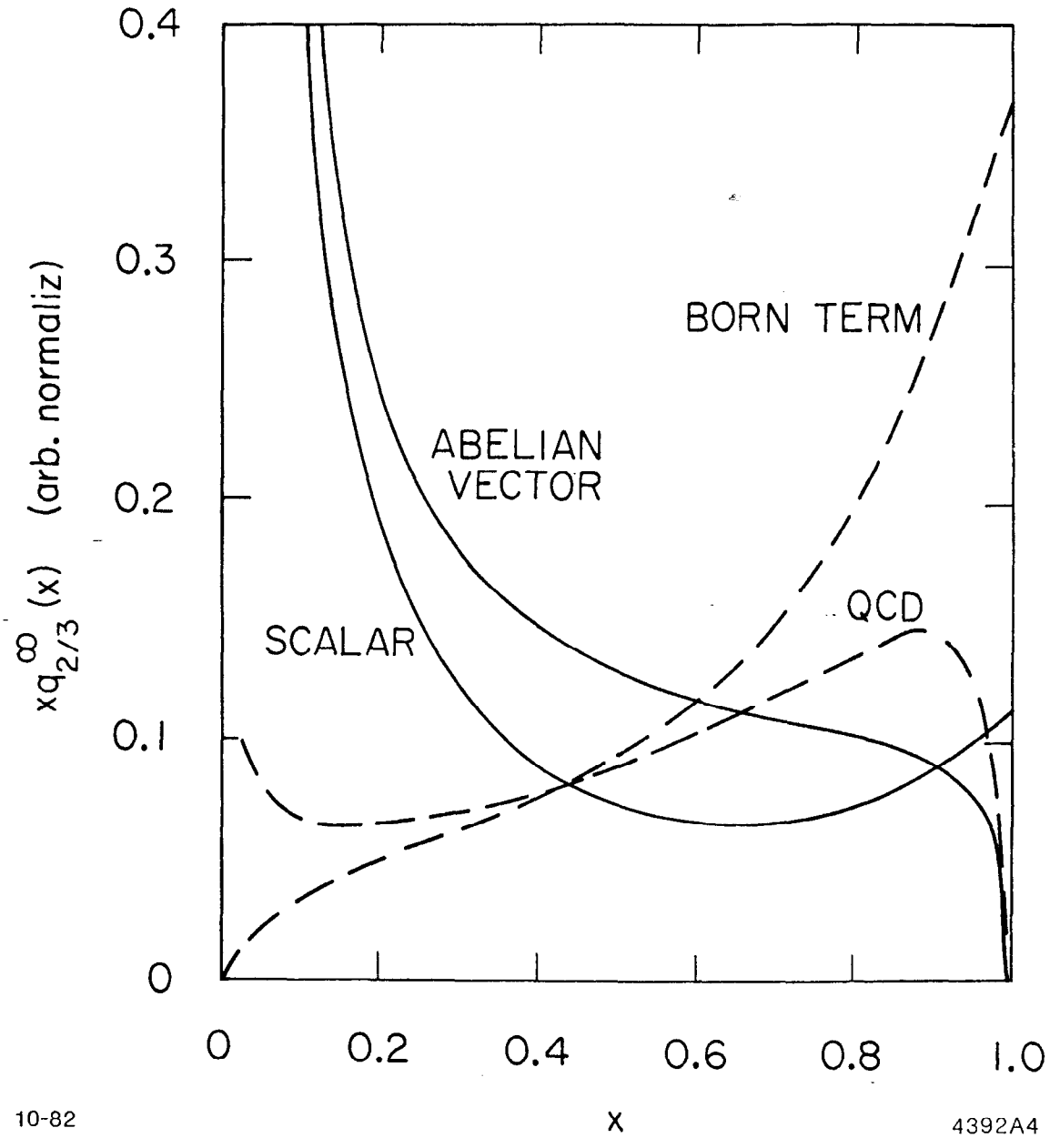
0.4
0.3
0.2
0.1
0
$xq^{8}_{2/3}(x)$ (arb. normaliz)
BORN TERM
ABELIAN VECTOR
QCD
SCALAR
0
0.2
0.4
0.6
0.8
1.0
X
10-82
4392A4

Fig. 4

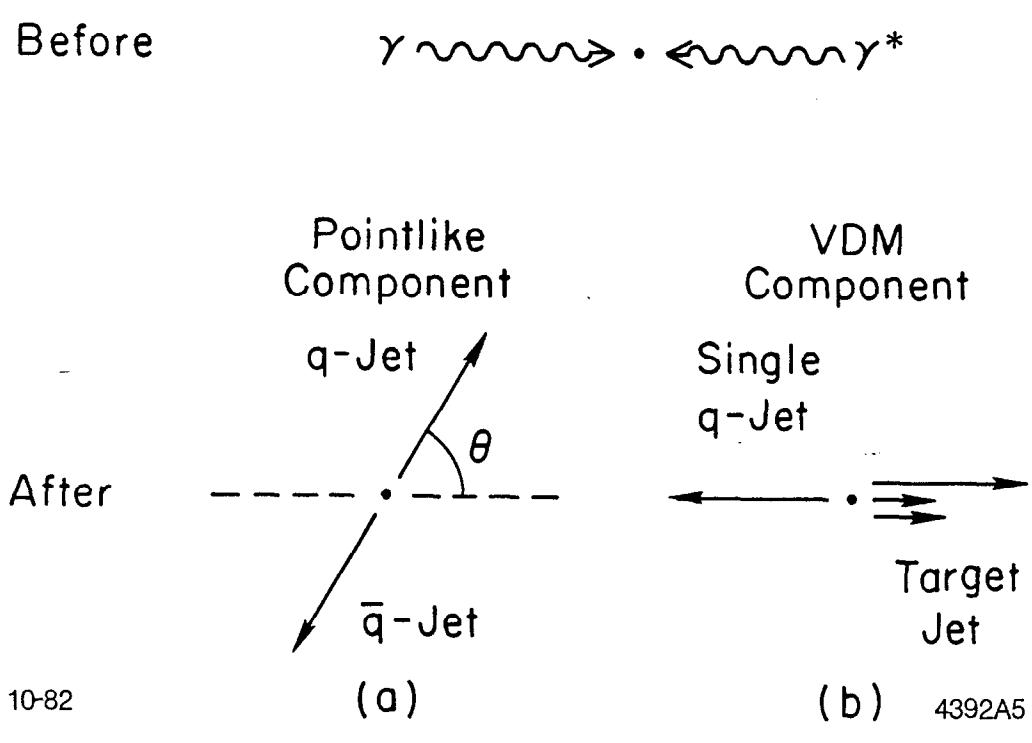
Before
γ
γ*
Pointlike
Component
VDM
Component
q-Jet
Single
q-Jet
θ
After
Target
Jet
q̄-Jet
10-82
(a)
(b)
4392A5

Fig. 5

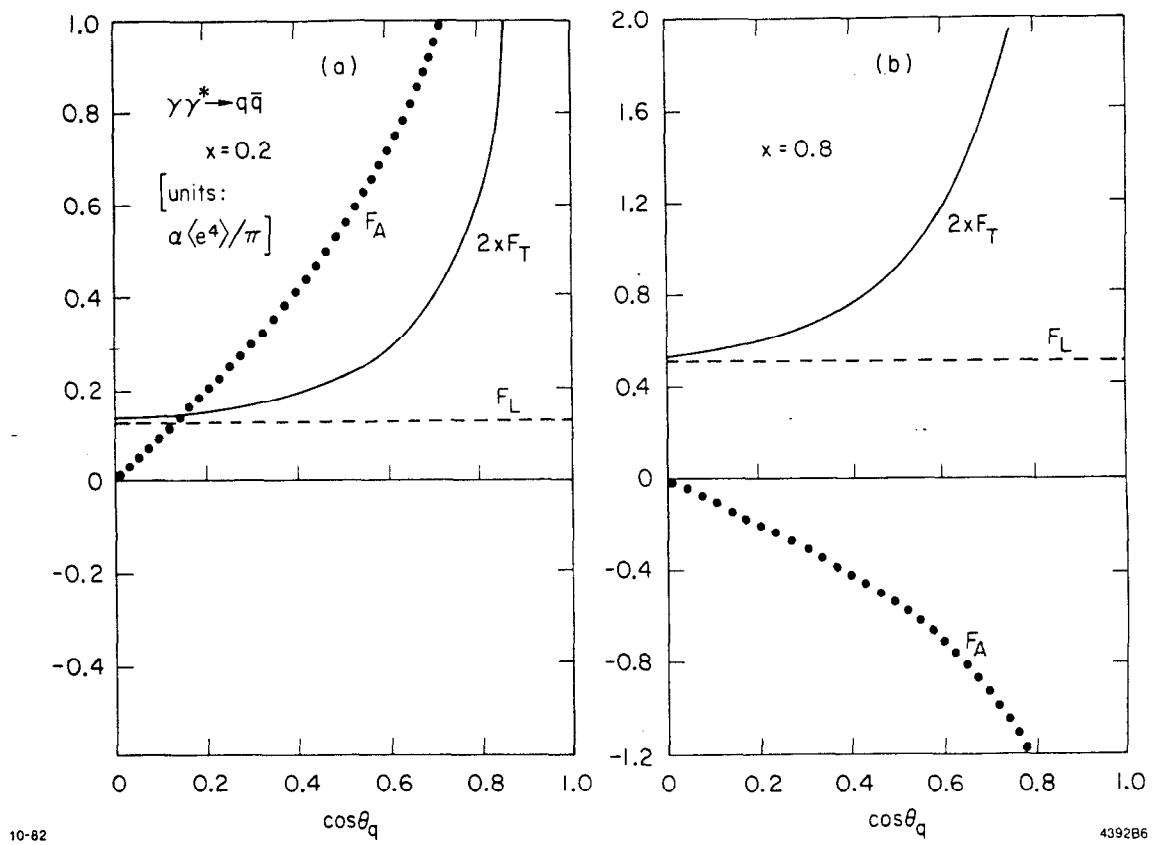
(a)
$\gamma\gamma^* \to q\bar{q}$
x = 0.2
[units:
$\alpha\langle e^4\rangle/\pi$]
F_A
$2xF_T$
F_L
(b)
x = 0.8
$2xF_T$
F_L
F_A
$\cos\theta_q$
$\cos\theta_q$
10-82
4392B6

Fig. 6

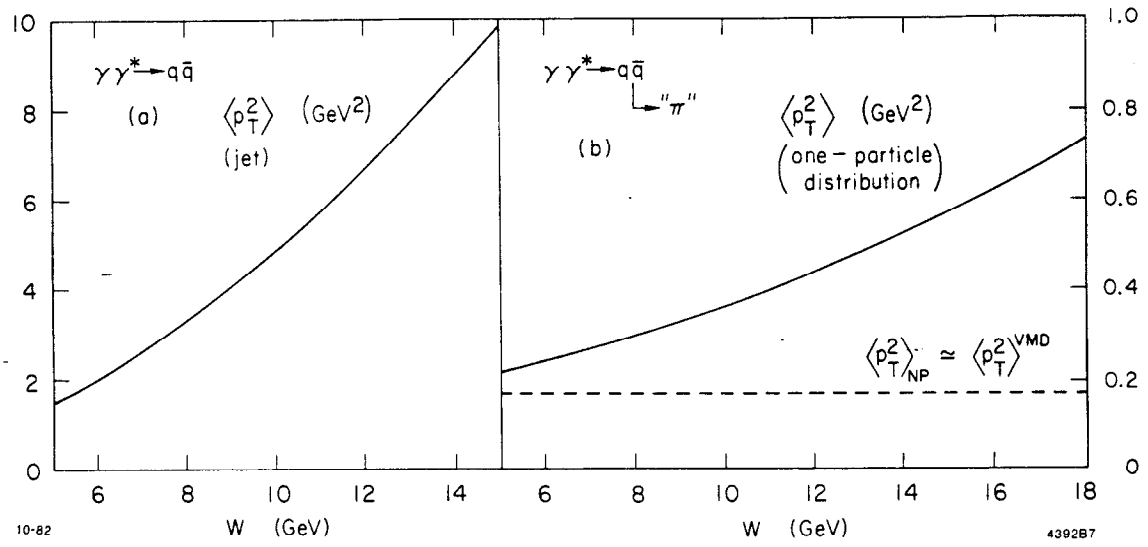
10
8
6
4
2
0
1.0
0.8
0.6
0.4
0.2
0
$\gamma\gamma^* \to q\bar{q}$
(a)
$\langle p_T^2 \rangle$ (GeV^2)
(jet)
$\gamma\gamma^* \to q\bar{q}$
"π"
(b)
$\langle p_T^2 \rangle$ (GeV^2)
(one − particle distribution)
$\langle p_T^2 \rangle_{NP} \simeq \langle p_T^2 \rangle^{VMD}$
6
8
10
12
14
16
18
W (GeV)
W (GeV)
10-82
4392B7

Fig. 7

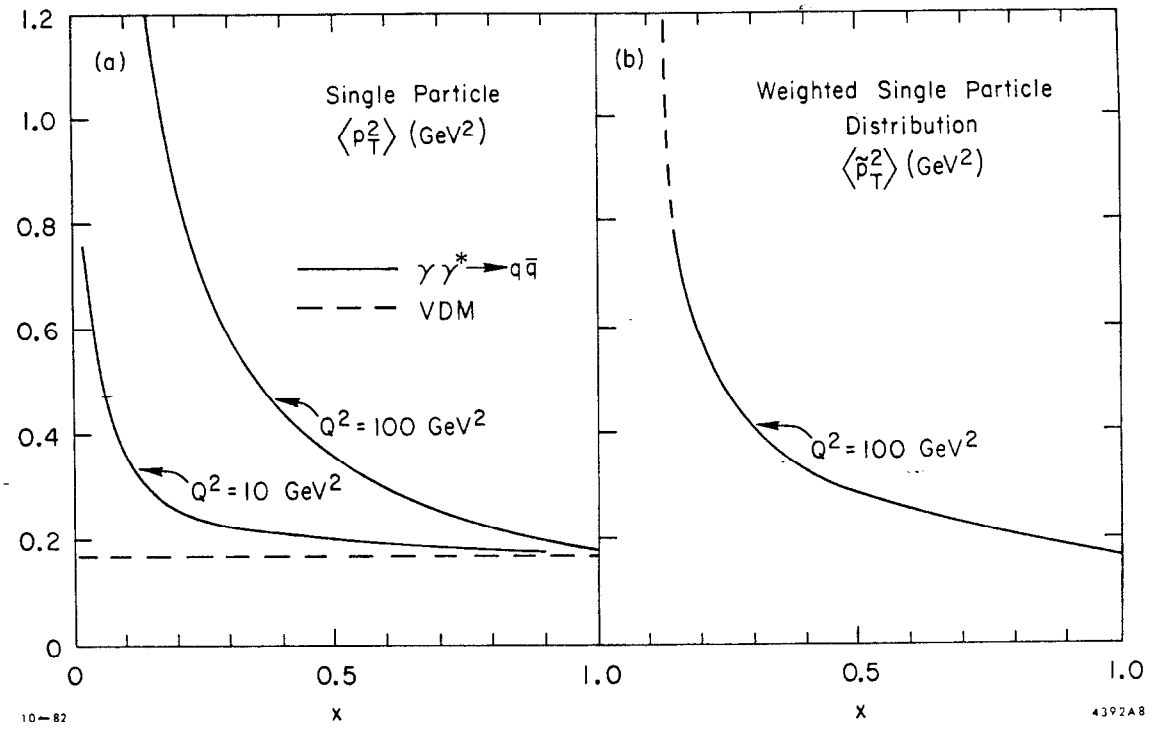
(a)
Single Particle
$\langle p_T^2 \rangle$ (GeV^2)
$\gamma\gamma^* \to q\bar{q}$
VDM
$Q^2 = 100$ GeV^2
$Q^2 = 10$ GeV^2
(b)
Weighted Single Particle
Distribution
$\langle \tilde{p}_T^2 \rangle$ (GeV^2)
$Q^2 = 100$ GeV^2
1.2
1.0
0.8
0.6
0.4
0.2
0
0
0.5
1.0
x
0.5
1.0
x
10—82
4392A8

Fig. 8